miR-30a Remodels Subcutaneous Adipose Tissue Inflammation to Improve Insulin Sensitivity in Obesity

Eun-Hee Koh,[1,2] Natasha Chernis,[1,3] Pradip K. Saha,[1,3] Liuling Xiao,[4] David A. Bader,[1] Bokai Zhu,[1] Kimal Rajapakshe,[1,5] Mark P. Hamilton,[1] Xia Liu,[1] Dimuthu Perera,[1,5] Xi Chen,[1] Brian York,[1] Michael Trauner,[6] Cristian Coarfa,[1,5] Mandeep Bajaj,[3] David D. Moore,[1] Tuo Deng,[4,7] Sean E. McGuire,[1,8] and Sean M. Hartig[1,3]

Diabetes 2018;67:2541–2553 | https://doi.org/10.2337/db17-1378

Chronic inflammation accompanies obesity and limits subcutaneous white adipose tissue (WAT) expandability, accelerating the development of insulin resistance and type 2 diabetes mellitus. MicroRNAs (miRNAs) influence expression of many metabolic genes in fat cells, but physiological roles in WAT remain poorly characterized. Here, we report that expression of the miRNA *miR-30a* in subcutaneous WAT corresponds with insulin sensitivity in obese mice and humans. To examine the hypothesis that restoration of *miR-30a* expression in WAT improves insulin sensitivity, we injected adenovirus (Adv) expressing *miR-30a* into the subcutaneous fat pad of diabetic mice. Exogenous *miR-30a* expression in the subcutaneous WAT depot of obese mice coupled improved insulin sensitivity and increased energy expenditure with decreased ectopic fat deposition in the liver and reduced WAT inflammation. High-throughput proteomic profiling and RNA-Seq suggested that *miR-30a* targets the transcription factor STAT1 to limit the actions of the proinflammatory cytokine interferon-γ (IFN-γ) that would otherwise restrict WAT expansion and decrease insulin sensitivity. We further demonstrated that *miR-30a* opposes the actions of IFN-γ, suggesting an important role for *miR-30a* in defending adipocytes against proinflammatory cytokines that reduce peripheral insulin sensitivity. Together, our data identify a critical molecular signaling axis, elements of which are involved in uncoupling obesity from metabolic dysfunction.

Excess body weight is an established risk factor for developing metabolic diseases, including type 2 diabetes mellitus (T2DM). However, ∼30% of obese individuals retain clinically normal measures of metabolic function characterized by insulin sensitivity (1,2). Although the molecular underpinnings that lead to insulin-sensitive obesity are not defined, the condition is linked to expansion of subcutaneous white adipose tissue (WAT) depots that efficiently sequester excess energy. Additionally, subcutaneous WAT expansion correlates with reduced incidence of obesity-linked conditions, including hepatic steatosis and T2DM (3–5). Therefore, factors that preserve the metabolic function of subcutaneous WAT may protect against the comorbidities of obesity.

Obesity is associated with chronic low-grade inflammation, reflecting significant alterations in the composition of immune cell populations that reside in WAT. The ensuing proinflammatory environment likely impinges on the

[1]Department of Molecular and Cellular Biology, Baylor College of Medicine, Houston, TX
[2]Department of Internal Medicine, University of Ulsan College of Medicine, Seoul, Republic of Korea
[3]Division of Diabetes, Endocrinology, and Metabolism, Department of Medicine, Baylor College of Medicine, Houston, TX
[4]Center for Bioenergetics, Houston Methodist Research Institute, Weill Cornell Medical College, Houston, TX
[5]Dan L. Duncan Comprehensive Cancer Center, Baylor College of Medicine, Houston, TX
[6]Hans Popper Laboratory of Molecular Hepatology, Division of Gastroenterology and Hepatology, Department of Internal Medicine III, Medical University of Vienna, Vienna, Austria
[7]Department of Metabolism and Endocrinology, The Second Xiangya Hospital and Key Laboratory of Diabetes Immunology (Central South University), Ministry of Education, Changsha, China
[8]Department of Radiation Oncology, The University of Texas MD Anderson Cancer Center, Houston, TX

Corresponding author: Sean M. Hartig, hartig@bcm.edu.

Received 15 November 2017 and accepted 3 July 2018.

This article contains Supplementary Data online at http://diabetes.diabetesjournals.org/lookup/suppl/doi:10.2337/db17-1378/-/DC1.

metabolic functions of adipocytes and may partially explain the insulin resistance that characterizes T2DM (6). Supporting these observations, proinflammatory cytokines, such as interferon-γ (IFN-γ) and tumor necrosis factor-α, correlate with insulin resistance, attenuated subcutaneous WAT expansion, and pathological central (visceral) WAT accumulation (7–10). WAT inflammation links obesity to insulin resistance and T2DM, but numerous questions remain unanswered, including how to sustain noninflamed subcutaneous WAT expansion during overnutrition.

Adipose tissue–specific microRNAs (miRNAs) influence metabolism by regulating adipocyte differentiation, inflammation, and metabolic functions (11). In an effort to discover new regulators of fatty acid metabolism, we recently discovered that the miRNA *miR-30a* regulates mitochondrial respiration in human adipocytes (12). *miR-30a* likely exerts this function by modulating an integrated gene program to increase expression of insulin sensitivity genes and elevate oxidative metabolism in white adipocytes. Here, we demonstrate that enforced *miR-30a* expression in the subcutaneous fat pads of diabetic mice robustly increases insulin sensitivity without affecting body weight. We establish that *miR-30a* expression is anti-inflammatory in adipocytes, and this effect occurs through direct suppression of the STAT1 signaling pathway. STAT1 activation reciprocally inhibits *miR-30a* expression in adipocytes, which likely contributes to the chronic inflammatory state of obesity. We conclude that *miR-30a* is a critical effector of subcutaneous WAT expansion and the inflammatory response associated with obesity.

RESEARCH DESIGN AND METHODS

Animal Care and Use

Diet-induced obesity (DIO) mice (The Jackson Laboratory) were fed 60% high-fat diet (HFD; Bio-Serv) for 12–14 weeks before experiments. Mouse body composition was examined by MRI (Echo Medical Systems). We obtained adenovirus (Adv) miR-control (m009), Adv-miR-30a (mm0332), Adv-anti-miR-control (m010), and Adv-miR-anti-miR-30a (m5539) from Applied Biological Materials, Inc. Adv (5×10^9 pfu/mL) was injected into both left and right inguinal fat pads of male DIO mice under anesthesia. At the end of experiments, tissues were collected, flash frozen in liquid N_2, and stored at −80°C until use.

Human Subjects

Cohort 1

Subcutaneous WAT biopsies (13) from the lateral thigh were obtained from obese subjects (BMI = 38.3 ± 1.5 kg/m^2, fasting plasma glucose = 82 ± 3 mg/dL, HOMA of insulin resistance [HOMA-IR] = 2.2 ± 0.3) and patients with recently diagnosed T2DM (BMI = 35.2 ± 3.8 kg/m^2, fasting plasma glucose = 126 ± 31 mg/dL, HOMA-IR 7.8 ± 2.1). All participants provided written informed consent.

Cohort 2

Subcutaneous WAT biopsies were obtained from obese subjects during gastric bypass surgery (14). Three subjects were defined as insulin sensitive (BMI = 37.7 ± 0.3 kg/m^2, fasting plasma glucose = 95.1 ± 3 mg/dL, HOMA-IR = 2.1 ± 0.2), and 12 patients were insulin resistant (BMI = 40.6 ± 1.0 kg/m^2, fasting plasma glucose = 99 ± 2 mg/dL, HOMA-IR = 5.8 ± 0.7).

The use of medications known to affect metabolism, particularly lipid- or glucose-lowering drugs, was an exclusion criterion in this study. Samples were stored at −80°C until RNA extraction. In both cohorts, the cutoff to separate insulin-sensitive and insulin-resistant patients was a HOMA-IR index of 2.

Antibodies and Immunoblotting

Western blotting was performed as previously described (12). Antibodies are listed in Supplementary Table 2.

Glucose and Insulin Tolerance Tests

To determine glucose tolerance, mice were fasted for 16 h and glucose was administered (1 g/kg body weight) by intraperitoneal injection. To determine insulin tolerance, mice were fasted for 6 h prior to intraperitoneal insulin (0.5 units/kg body weight). Blood glucose levels were measured by handheld glucometer.

Metabolic Cages

Energy expenditure studies were conducted using Oxymax System cages (Columbus Instruments, Columbus, OH). Mice were acclimated in the metabolic chambers for 3 days before the start of experiments. Food intake, heat production, and CO_2 and O_2 levels were measured over 12-h light and 12-h dark cycles for a total of 4 days.

FACS Analysis of Inguinal WAT Stromal Vascular Fraction

Minced adipose tissue was placed in digestion buffer containing 0.5% BSA and 1 mg/mL collagenase (catalog no. C2139; Sigma-Aldrich) and incubated in a 37°C shaking water bath for 30 min. The mixture was passed through a 100-μm filter before low-speed centrifugation. Erythrocytes were removed from the stromal vascular fraction (SVF) pellet with RBC Lysis Buffer (catalog no. 420301; BioLegend). The purified SVF pellet was resuspended in FACS buffer, incubated with Fc Block (catalog no. 14-0161-85; eBioscience), and stained with conjugated antibodies. The following antibodies were used for FACS: CD45 (catalog no. 12-0481-82; eBioscience), F4/80 (catalog no. 123113; BioLegend), CD11b (catalog no. 101227; BioLegend), and CD11c (catalog no. 48-0114-82; eBioscience). Stained cells were washed twice in PBS and fixed in 1% formaldehyde before analysis. Samples were profiled using a LSRII cytometer (Becton Dickinson) coupled with FACS Diva (BD Biosciences) and FlowJo (Tree Star) software.

Real-time PCR and Chromatin Immunoprecipitation

Total RNA was extracted using the Direct-zol RNA MiniPrep Kit (Zymo Research). Primer sequences and gene expression assays are detailed in Supplementary Tables 3 and 4.

miR-30a Expression Analysis

The TaqMan Advanced miRNA cDNA Synthesis Kit (catalog no. A28007; Thermo Fisher) was used to synthesize

miR-30a-5p cDNA from total RNA. To extend mature miRNAs, polyadenylation and adaptor sequence ligation of the 3′ and 5′ ends, respectively, occur prior to universal priming and reverse transcription. To address low-expressing targets, cDNA is amplified by primers that recognize sequences appended to both ends, effectively minimizing amplification bias. TaqMan Advanced miRNA Assays (catalog no. A25576; Thermo Fisher) were used to quantify relative gene expression. Invariant RNA controls included *sno412* (mouse), *RNU48* (human), *let-7g-5p*, and *miR-423-5p*.

Reverse-Phase Protein Array

Protein lysates were prepared with Tissue Protein Extraction Reagent (Thermo Fisher) containing protease and phosphatase inhibitors (Roche). The Aushon 2470 Arrayer (Aushon BioSystems) with a 40 pin (185 μm) configuration was used to spot lysates onto nitrocellulose-coated slides (Grace Bio-Labs). The slides were probed with 220 antibodies against total and phosphoprotein proteins using an automated slide stainer (Dako). Primary antibody binding was detected using a biotinylated secondary antibody followed by streptavidin-conjugated IRDye 680 fluorophore (LI-COR Biosciences). Fluorescent-labeled slides were scanned on a GenePix AL4200, and the images were analyzed with GenePix Pro 7.0 (Molecular Devices). Total fluorescence intensities of each spot were normalized for variation in total protein (Sypro Ruby) and nonspecific labeling.

RNA-Seq

Poly-A RNA was purified from total RNA using Dynabeads Oligo dT25 (Invitrogen) and fragmented for size selection. First-strand cDNA was synthesized using Superscript Reverse Transcriptase III (Invitrogen). Second-strand cDNA was synthesized and marked with dUTP. The resultant cDNA was used for end repair, A-tailing, and adaptor ligation. The second-strand cDNA was then degraded by Uracil-DNA Glycosylase (NEB) and the library was amplified for sequencing (Illumina HiSeq2000). Read pairs were mapped using TopHat2 (15) onto the UCSC mouse genome (mm10) and RefSeq compendium of genes. Gene expression was computed using Cufflinks2 (16). Gene set enrichment analysis (GSEA) was performed with DAVID against the Kyoto Encyclopedia of Genes and Genomes (KEGG) database. The RNA-Seq data set can be accessed at the Gene Expression Omnibus (GSE39342).

Statistical Analyses

Statistical significance was assessed by unpaired Student *t* test. All tests were performed at the 95% CI. Pearson correlation coefficient (Pearson *r*) was calculated to evaluate correlations between metabolic parameters and *miR-30a* expression in human subcutaneous WAT. Detailed methods are provided in the Supplementary Data.

Study Approval

All animal procedures were approved by the Baylor College of Medicine Institutional Animal Care and Use Committee. Human studies were approved by the ethics committee at Karolinska Institutet (Dnr 2008/2:3) and the Baylor College of Medicine Institutional Review Board (H-28439).

RESULTS

miR-30a Expression in Adipose Tissue Correlates With Insulin Sensitivity

miR-30a regulates transcription of genes important for lipid metabolism in human adipocytes (12) and favorably correlates with multiple insulin-sensitive phenotypes analyzed in the Metabolic Syndrome in Men (METSIM) study (17). To explore the hypothesis that *miR-30a* expression in WAT corresponds with insulin sensitivity, we measured *miR-30a* levels in fat tissues collected from insulin-resistant mice and humans. *miR-30a* expression was reduced in subcutaneous WAT isolated from DIO mice compared with mice fed normal chow (Fig. 1*A*). In obese humans (13), *miR-30a* was 40% lower in subcutaneous WAT isolated from insulin-resistant subjects compared with normoglycemic counterparts (Fig. 1*B*). Further, *miR-30a* levels were inversely correlated with measures of insulin resistance (Fig. 1*C*), including HOMA-IR ($Pr = -0.56$, $P = 0.008$). These results suggest that decreased *miR-30a* expression is associated with compromised fat cell function in the context of insulin resistance, but not obesity.

miR-30a Overexpression in Subcutaneous Fat Improves Insulin Sensitivity

To determine if restoring *miR-30a* expression could improve adipocyte function in insulin-resistant mice, we injected the inguinal fat pad of DIO mice with an Adv expressing *miR-30a* or GFP (Fig. 2*A*). The GFP reporter present in both constructs allowed us to confirm infection efficiency by immunohistochemistry (Supplementary Fig. 1*A*) and flow cytometry (Supplementary Fig. 1*B*). After 7 days, we detected threefold higher expression of *miR-30a* compared with the GFP control in the inguinal fat pad

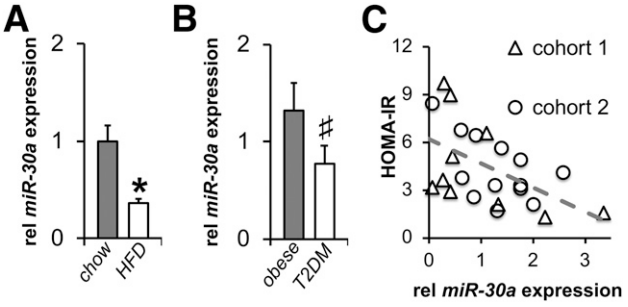

Figure 1—*miR-30a* expression in adipose tissue correlates with insulin sensitivity. *A*: qPCR was used to determine *miR-30a* expression levels in subcutaneous WAT isolated from male mice fed chow or HFD. Mice were fed chow or HFD for 12 weeks ($n = 6$/group). *$P < 0.05$. *B*: Relative *miR-30a* expression was measured in subcutaneous adipose tissue biopsied from obese ($n = 12$) and obese T2DM ($n = 9$) subjects. #$P < 0.06$. Data are represented as mean ± SEM. *C*: *miR-30a* expression is negatively correlated with HOMA-IR in human subjects.

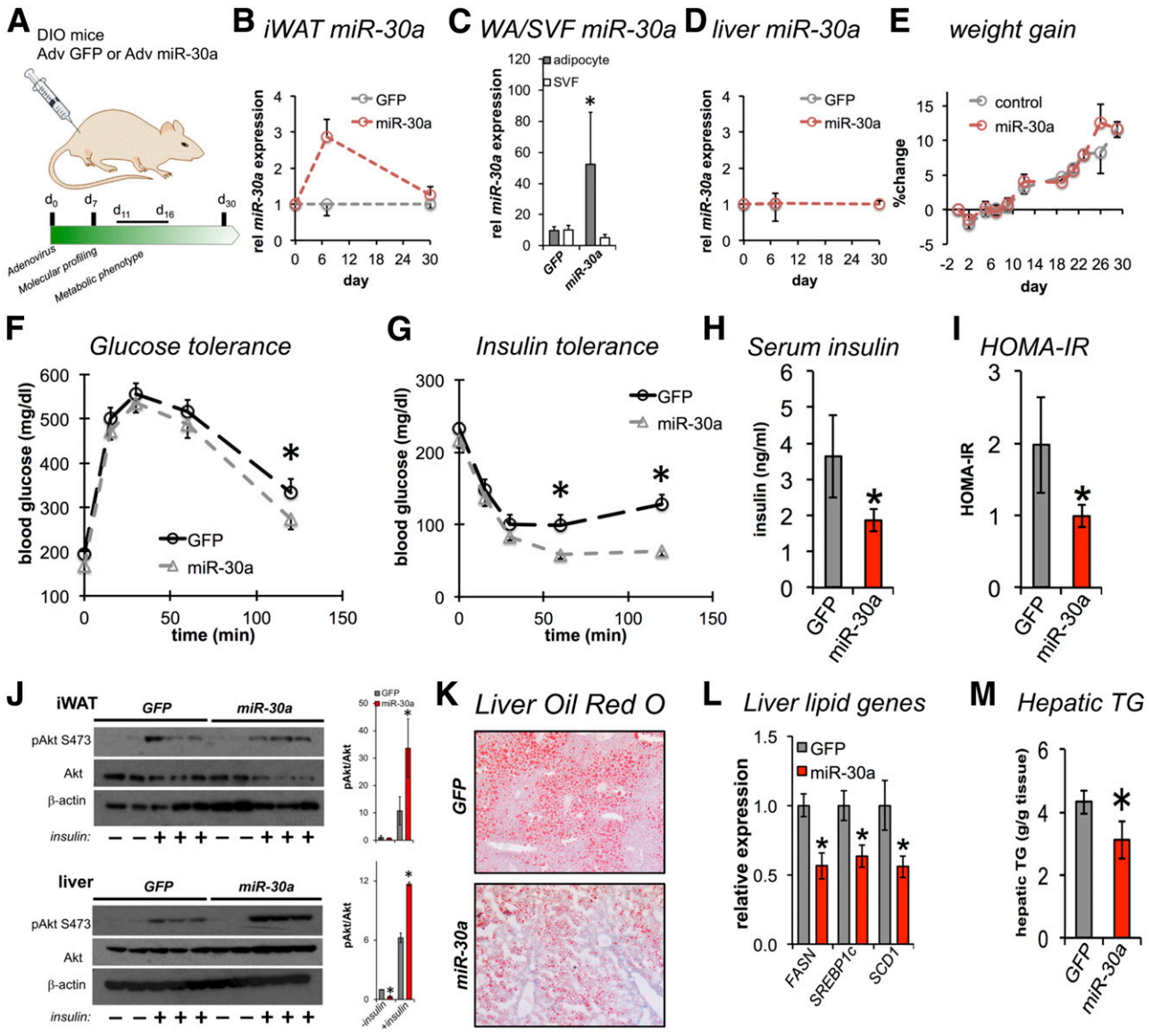

Figure 2— Ectopic miR-30a expression in subcutaneous WAT improves insulin sensitivity. *A*: Adv-GFP or Adv-miR-30a was injected into the inguinal fat pad of DIO mice fed HFD for 16 weeks. *miR-30a* expression levels were confirmed using RNA (n = 5) isolated from iWAT (*B*), stromal vascular and adipocyte (WA) fractions (*C*), and liver (*D*). *E*: Body weight gain (% initial) was measured during ectopic miR-30a in iWAT. Two weeks after the initial injection, glucose metabolism was determined by glucose tolerance (*F*) and insulin tolerance (*G*) tests (n = 12 mice/group). Serum insulin levels (*H*) and HOMA-IR (*I*) were assessed in fasted mice (4 h) injected with Adv-miR-30a or Adv-GFP control (n = 12 mice/group). *J*: Mice expressing Adv-miR-30a or Adv-GFP in iWAT were fasted 4 h and tissues collected 10 min after PBS or insulin (0.5 units/kg). Western blot analysis and relative protein levels for pAkt (S473) and total Akt in iWAT and liver lysates. *K*: Liver sections were stained with Oil Red O to examine the effects of iWAT miR-30a overexpression in liver fat. *L*: qPCR was used to determine the expression of lipogenic genes in the liver. *M*: Reduced fat content in the liver was confirmed by measurement of hepatic triglycerides (TG). All data are expressed as mean ± SEM (n = 5). *$P < 0.05$.

(Fig. 2*B*). To specifically quantify *miR-30a* expression in fat cells, we separated adipocytes from the SVF. *miR-30a* levels were almost sixfold higher (5.4×) in the adipocyte fraction of DIO mice ectopically expressing Adv-miR-30a in the inguinal WAT (iWAT) compared with the control treatment group (Fig. 2*C*). Importantly, liver *miR-30a* expression was unaffected after adipose tissue infections (Fig. 2*D*).

Contrary to our expectations, weight gain on HFD was unchanged after Adv-miR-30a or GFP transgenesis (Fig. 2*E*). Although glucose tolerance was modestly improved by miR-30a expression in subcutaneous WAT (Fig. 2*F*), this treatment was sufficient to markedly enhance insulin sensitivity (Fig. 2*G*) and reduce serum insulin levels (Fig. 2*H*). Likewise, the HOMA-IR (Fig. 2*I*) was significantly decreased, suggesting that ectopic miR-30a expression in subcutaneous WAT improves insulin sensitivity in obese mice. We next asked whether insulin sensitivity changes in DIO mice expressing Adv-miR-30a in iWAT were reflected in improved insulin signaling. Indeed, Adv-miR-30a expression in subcutaneous WAT increased insulin-dependent phosphorylation of Akt at S473 in the iWAT and liver (Fig. 2*J*). Serum triglyceride (Supplementary Fig. 2*A*), free

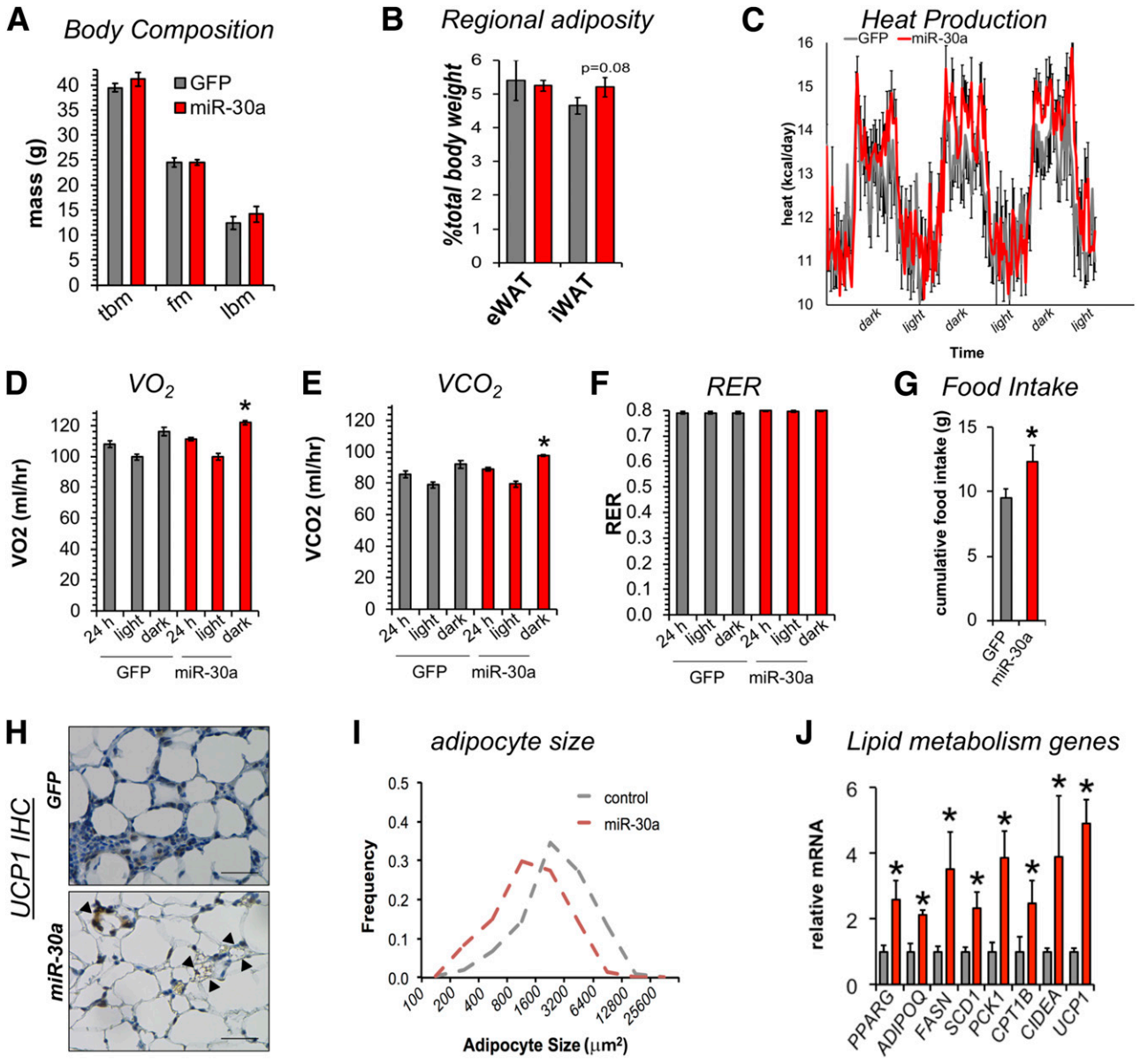

Figure 3—miR-30a expression in iWAT of DIO mice improves energy balance. Body composition (*A*) and fat depot mass (normalized to body weight) (*B*) of DIO mice ectopically expressing Adv-GFP or Adv-miR-30a in iWAT. *C*: Energy expenditure (heat) during two complete 12-h light-dark cycles 11 days after local expression of Adv-GFP or Adv-miR-30a in iWAT of DIO mice. Average oxygen consumption (VO_2) (*D*), carbon dioxide production (VCO_2) (*E*), and respiratory exchange ratio (RER) (*F*) during the 12-h light-dark cycles were determined by Comprehensive Lab Animal Monitoring System (CLAMS). *G*: Cumulative food intake during CLAMS experiments ($n = 5$). *H*: Histology showing UCP1 immunostaining in iWAT of Adv-GFP or Adv-miR-30a DIO mice. Arrowheads indicate UCP1-positive cells. Scale bars, 50 μm. Adv-miR-30a expression in iWAT remodels adipocyte size (*I*) and restores expression of lipid metabolism genes (*J*) ($n \geq 4$). All data are expressed as mean ± SEM. $^*P < 0.05$. All metabolic cage measurements are presented on a per mouse basis. eWAT, epididymal WAT; fm, fat mass; IHC, immunohistochemistry; lbm, lean body mass; tbm, total body mass.

fatty acid (Supplementary Fig. 2*B*), and cholesterol (Supplementary Fig. 2*C*) levels were also reduced by Adv-miR-30a expression in subcutaneous WAT of DIO mice. Histological examination of liver lipid content by Oil Red O staining showed that miR-30a overexpression in subcutaneous fat decreased hepatic steatosis (Fig. 2*K*). In agreement with reduced liver fat, expression of genes associated with de novo lipogenesis was decreased (Fig. 2*L*), as was the level of hepatic triglycerides (Fig. 2*M*). Together, these data suggested that miR-30a expression in subcutaneous WAT influences systemic insulin sensitivity and circulating lipid parameters without altering body weight.

miR-30a Expression in Subcutaneous WAT Confers Improved Energy Expenditure

To further define the metabolic phenotype of ectopic miR-30a expression in iWAT, we performed comprehensive analysis of body composition and energy expenditure.

At the time of analysis (11 days after injection), we did not observe a significant difference in body composition (Fig. 3*A*) or fat distribution (Fig. 3*B*). However, we detected a modest, but statistically significant, increase in heat production (Fig. 3*C*), O_2 consumption (Fig. 3*D*), and CO_2 production (Fig. 3*E*) during the night phase in the DIO mice injected with Adv-miR-30a. Carbohydrate and fat usage estimated by the respiratory exchange ratio was similar between Adv-GFP and Adv-miR-30a treatment groups (Fig. 3*F*). The absence of a body weight difference between Adv-GFP and Adv-miR-30a treatments could be attributed to greater food intake (Fig. 3*G*) offset by elevated energy expenditure.

Recruitment of UCP1-positive adipocytes affects energy expenditure in rodents (18). Our previous findings (12) suggested that Adv-miR-30a injection into the inguinal fat pad may influence changes in UCP1 expression that ultimately impact energy balance. Consistent with this notion, the appearance of UCP1-positive cells in iWAT accompanied the energy expenditure changes induced by Adv-miR-30a injection (Fig. 3*H*). The energy expenditure effects we observed corresponded with smaller adipocyte size (Fig. 3*I*), which in turn correlates with WAT hyperplasia and insulin sensitivity (19). As expected, WAT-specific genes (12), including *ADIPOQ*, and other lipid metabolism genes (*SCD1*, *PCK1*, and *CPT1B*) were highly induced by Adv-miR-30a transgenesis (Fig. 3*J*). Notably, induction of UCP1 was selectively enhanced over classic white adipocyte genes such as *ADIPOQ* (2.3×), which supported data demonstrating that the effects of Adv-miR-30a in iWAT were not due to primary effects on adipogenesis in vivo (Supplementary Fig. 3*A*) or in vitro (Supplementary Fig. 3*B*). Rather, transfection of miR-30a mimics into mature human adipocytes changed fat cell properties in a manner similar to rosiglitazone. Two days after transfection, we found that miR-30a mimic promotes lipid droplet biogenesis and mitochondrial protein expression (Supplementary Fig. 4*A*) concurrent with significantly elevated markers of fat metabolism (Supplementary Fig. 4*B*). These data argue that acquisition of brown-like features in white adipocytes contributes to the metabolic phenotype enforced by *miR-30a* expression in iWAT.

miR-30a Ablates Diet-Induced Subcutaneous Adipose Tissue Inflammation

During sustained HFD feeding, obesity initiates low-grade metabolic inflammation that ultimately coincides with insulin resistance and T2DM. In this setting, WAT harbors macrophages that play a critical role in chronic inflammation and metabolic dysfunction (20,21). To determine whether Adv-miR-30a affected macrophage infiltration in adipose tissues, we examined histological sections of iWAT. *miR-30a* expression repressed proinflammatory macrophage infiltration (Fig. 4*A*), but it had no effect on the abundance of resident tissue macrophages (Supplementary Fig. 5*A*) or the broad expression of genes (Supplementary Fig. 5*B*) that specify adipocyte identity and proinflammatory responses in epididymal WAT.

To characterize cell signaling events underpinning this observation, we applied the samples to a reverse-phase protein array (RPPA) with broad pathway coverage (Fig. 4*B*). Mice injected with Adv-miR-30a exhibited suppressed protein expression of published *miR-30a* targets that correspond with insulin resistance and impaired mitochondrial function, including Ubc9 (12), ATG12 (22,23), and BECN1 (24), which broadly coincided with higher UCP1 expression. Unexpectedly, RPPA analysis revealed that phospho-STAT1 (Y701) was markedly repressed in mice injected with Adv-miR-30a. Depletion of total STAT1 and phospho-STAT1 levels were confirmed by immunoblotting (Fig. 4*C*).

We next used RNA-Seq to identify global effects of Adv-miR-30a overexpression in subcutaneous WAT 7 days after infection. To further demonstrate that *miR-30a* expression in the subcutaneous WAT of DIO mice is associated with thermogenic adipocytes, we performed GSEA (25) using reference gene expression data sets (GSE39562) from brown and beige adipocyte cell lines (26). We found that genes affected by Adv-miR-30a expression were significantly enriched in beige (normalized enrichment score = 4.82) and brown (normalized enrichment score = 3.51) cells compared with white adipocytes (Supplementary Table 1*B*).

Gene ontology analysis suggested that Adv-miR-30a treatment is broadly anti-inflammatory, with evidence for suppression of toll-like receptor, chemokine, and JAK-STAT signaling (Fig. 4*D*). We individually validated several representative inflammatory genes, and all showed significant suppression by Adv-miR-30a expression in subcutaneous WAT (Fig. 4*E*). Flow cytometry analysis confirmed that Adv-miR-30a expression in subcutaneous WAT reduced inflammation derived from $F4/80^+CD11b^+$ macrophages (Fig. 4*F*). More specifically, Adv-miR-30a injection in iWAT depleted $CD11c^+$ cells, which are recognized as classically activated M1 macrophages (Fig. 4*G*). These results demonstrate that miR-30a overexpression results in reduced inflammation and the appearance of thermogenic adipocytes in subcutaneous WAT.

STAT1 Is a miR-30a Target in Adipocytes

We used the BROAD Molecular Signatures Database (mSigDB v4.0) to identify transcription factor programs underpinning the broad blockade of WAT inflammation by Adv-miR-30a. This analysis (Fig. 5*A*) revealed significant enrichment of transcription factors that cooperate with STAT1 (IFN-sensitive response element [ISRE]), including IFN response factors (IRFs). Consistent with this notion, direct targets with STAT1 binding sites ±2 kb from the transcription start site showed reduced mRNA expression by RNA-Seq and directed quantitative PCR (qPCR) analysis in subcutaneous WAT infected with Adv-miR-30a (Fig. 5*B*).

To investigate direct connections between *miR-30a* and STAT1, we used our database of miRNA-target binding inferred by high-throughput sequencing (27,28) and found

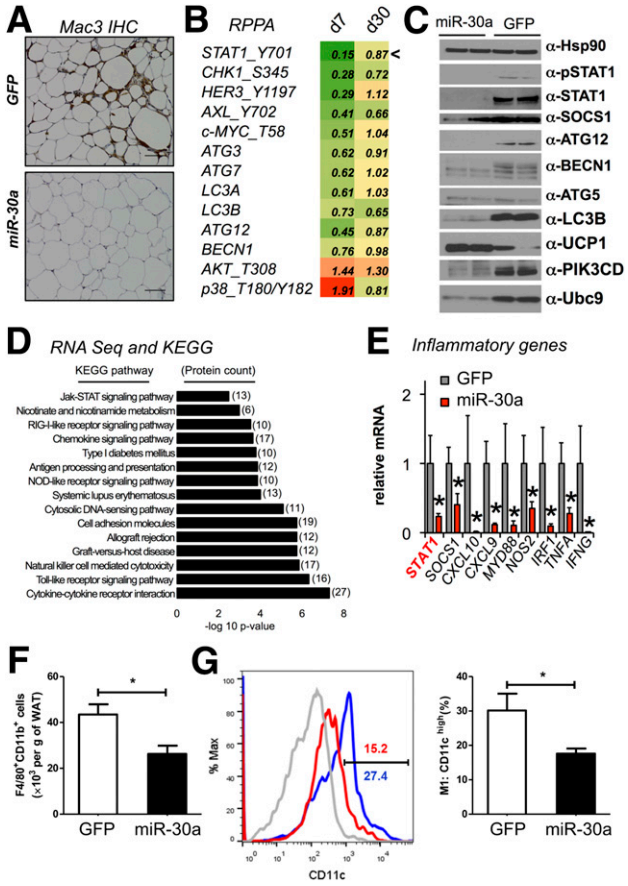

Figure 4—miR-30a ablates inflammation in the iWAT of diabetic mice. *A*: Immunohistochemistry (IHC) staining for resident proinflammatory macrophages in iWAT from DIO mice treated with local Adv-GFP or Adv-miR-30a injection. Scale bars, 50 μm. *B*: RPPA profiling performed 7 and 30 days after iWAT Adv-GFP or Adv-miR-30a injections. Antibody probes that show statistically significant change at 7 days are shown. Each column represents three mice per group. *C*: Western blotting with indicated antibodies to validate RPPA results or other miR-30a targets with independent iWAT lysates. *D*: RNA-Seq coupled with pathway analysis identified that inflammatory gene signatures are suppressed by ectopic Adv-miR-30a expression in subcutaneous WAT of DIO mice (574 genes total down, $P < 0.10$, $n = 4$/group). *E*: Relative mRNA expression of key genes that validate the anti-inflammatory signature of Adv-miR-30a in subcutaneous WAT ($n \geq 4$). Flow cytometry analysis to verify that Adv-miR-30a expression in iWAT reduces local F4/80$^+$ (*F*) and CD11c$^+$ M1 macrophage infiltration (*G*) ($n = 5$ mice/group). Red, Adv-miR-30a; blue, Adv-GFP; gray, isotype control ($n = 5$ mice/group). All data are expressed as mean ± SEM. *$P < 0.05$.

consistent targeting of the *STAT1* 3′-UTR by *miR-30a* in several cell lines (Fig. 5*C*). We then demonstrated *miR-30a* binding to the *STAT1* 3′-UTR by transiently coexpressing luciferase reporter fusions of *STAT1* and miRNA mimics in human adipocytes. Results from these cotransfection experiments indicated that the relative luciferase activity in *STAT1* 3′-UTR–expressing cells was significantly inhibited by *miR-30a*, whereas other 3′-UTR fusions that contained mutations (m1 and m2) in *miR-30a* binding sites were unaffected (Fig. 5*D*). Consistent with these findings and our Adv-miR-30a experiments in vivo, *miR-30a* overexpression in human adipocytes effectively decreased endogenous STAT1 mRNA, protein expression, and activity (Fig. 5*E*). Overall, these data suggest that STAT1 is a direct target of *miR-30a*.

We examined the functional role of the STAT1/*miR-30a* axis by performing phenotypic analyses of mature human adipocytes transfected with *STAT1* small interfering RNA (siRNA), *miR-30a* mimic, or appropriate controls. *STAT1* knockdown or *miR-30a* mimic (Fig. 5*F*) transfections produced a similar effect on metabolic and insulin sensitivity (*ADIPOQ*) genes, including significant induction of genes that mediate fatty acid handling (*FABP4*) and oxidation (*UCP1* and *PGC-1a*). Subsequent immunoblot analysis (Fig. 5*G*) confirmed that *STAT1* knockdown by siRNA or *miR-30a* mimic increased ADIPOQ, PRDM16, and UCP1 protein levels while augmenting expression of mitochondrial markers (cytochrome c [CytC] and Hsp60). We next measured oxygen consumption rates (OCRs) in the *miR-30a*–treated cells to determine the impact of these changes on metabolic activity. We found that knockdown of *STAT1* expression by siRNA or *miR-30a* mimic increased both oligomycin-insensitive and maximal respiration rates (Fig. 5*H*). STAT1 protein levels were fully depleted by combined siRNA and *miR-30a* knockdown, which corresponded to higher UCP1 expression (Supplementary Fig. 6*A*). Metabolic genes trended higher than single siRNA or miRNA mimic treatments, including prominent effects on *PRDM16*, *UCP1*, and *ADIPOQ* (Supplementary Fig. 6*B*). In contrast, individual siRNA or *miR-30a* transfections were sufficient to maximally suppress STAT1 target genes and mRNA expression of inflammatory cytokines (Supplementary Fig. 6*C*). Maximal OCR in cells was increased under combined blockade of STAT1 expression similar to single transfection conditions (Supplementary Fig. 6*D*). In sum, STAT1 inhibition by siRNA or *miR-30a* transfection yielded similar metabolic changes in human adipocytes that are unequivocally linked to improved insulin sensitivity.

Depletion of miR-30a Amplifies Adipose Tissue Inflammation

Our data suggested that *miR-30a* targets STAT1 directly in both mouse and human cells. To study the metabolic effect of *miR-30a* silencing, we injected Adv expressing anti-miR-30a directly into the inguinal adipose depot of lean mice fed HFD for 3 weeks. (Fig. 6*A*). At necropsy, repeated Adv-anti-miR-30a injections decreased *miR-30a* expression in iWAT by 30% (Fig. 6*B*). Although weight gain was unchanged (Fig. 6*C*), the loss of *miR-30a* in subcutaneous WAT decreased insulin sensitivity (Fig. 6*D*) coupled with a rise in both fasting insulin levels (Fig. 6*E*) and HOMA-IR (Fig. 6*F*). Consistent with reciprocal regulation of miR-30a and STAT1, the expression levels of STAT1 were increased in the iWAT of anti-miR-30a–treated mice (Fig. 6*G*). Further, *miR-30a* depletion significantly increased expression of STAT1 target genes, including *STAT1* itself, as well as the proinflammatory cytokines *TNFA* and *IFNG* (Fig. 6*H*). The proinflammatory response induced by anti-miR-30a was accompanied by decreased expression of genes

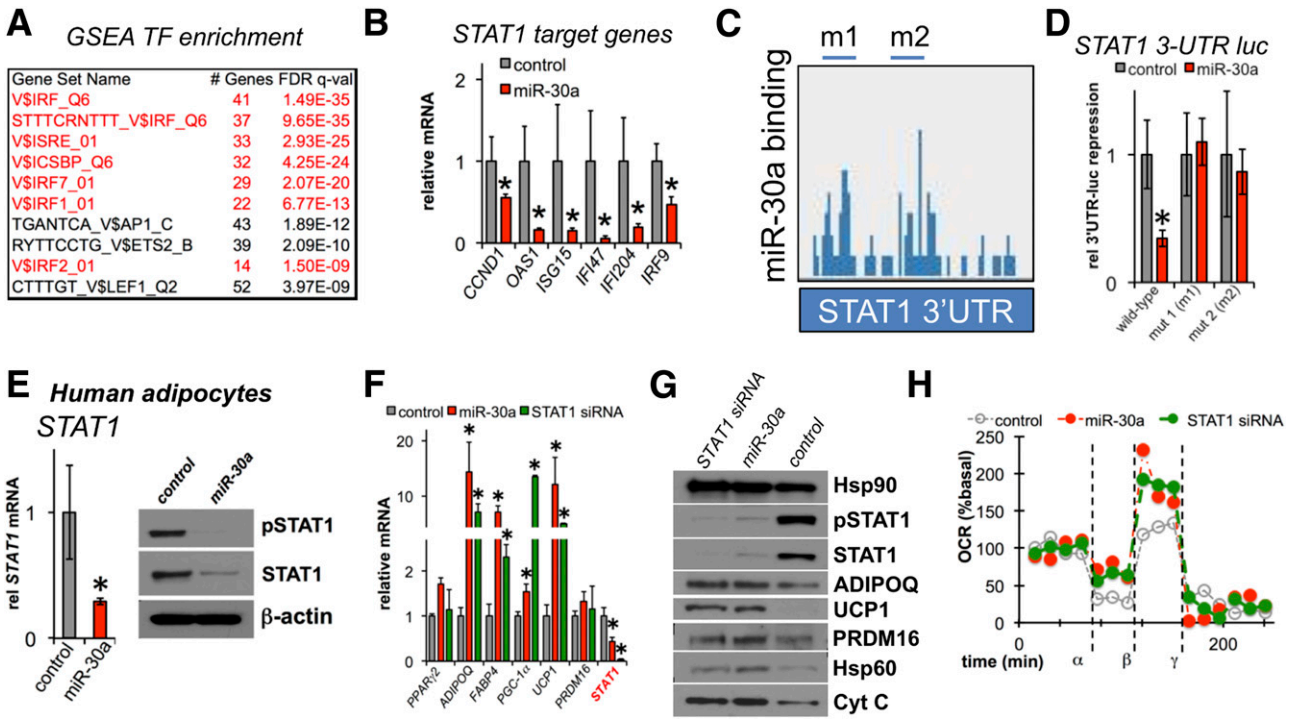

Figure 5—STAT1 is a target of miR-30a in adipocytes. *A*: Top enriched, miR-30a repressed gene sets from the GSEA using the MSigDB C3 transcription factor (TF) targets gene set collection. *B*: mRNA expression of STAT1 target genes in subcutaneous WAT expressing Adv-GFP or Adv-miR-30a. *C*: Bioinformatic analysis of AGO-CLIP experiments show that miR-30a binds to two sites within the 3-UTR of *STAT1*. *D*: STAT1 3-UTR luciferase fusions were coexpressed with control or miR-30a mimic in human adipocytes. m1, mutant 1; m2, mutant 2 (n = 3 independent experiments). *E*: STAT1 mRNA, total protein, and activation (pSTAT1 Y701) are suppressed by miR-30a mimic transfection in human adipocytes. *F*: *STAT1* siRNA, *miR-30a*, or transfection control was introduced into mature human adipocytes. The effects of *STAT1* siRNA and *miR-30a* overexpression in human adipocytes were characterized by qPCR analysis of *PPARγ2*, *ADIPOQ*, *FABP4*, *PGC1a*, *UCP1*, *PRDM16*, and *STAT1* mRNA levels ($n \geq 3$ independent experiments). *G*: Expression levels of pSTAT1 Y701, total STAT1, ADIPOQ, UCP1, PRDM16, Hsp60, and CytC were analyzed by immunoblotting for human adipocytes transfected with *STAT1* siRNA or a *miR-30a* mimic. *H*: Respiration (as OCR) was measured in human adipocytes transfected with *STAT1* siRNA, *miR-30a* mimic, or control oligomers. The OCR was measured over time with the addition of oligomycin (α), carbonyl cyanide-4-(trifluoromethoxy)phenylhydrazone (FCCP) (β), and anti–mycin-A/rotenone (γ). Percent change in OCR (%basal) was normalized to baseline rates (n = 5/group). *$P < 0.05$, relative to control transfection.

that support insulin sensitivity and lipid metabolism (Fig. 6*I*). Histological sections of iWAT stained with macrophage marker antibodies (Mac3) indicated that lower *miR-30a* levels were associated with increased proinflammatory macrophage infiltration (Fig. 6*J*). Moreover, adipocyte size was increased in the fat pads injected with anti-miR-30a, compared with controls (Fig. 6*K*). We also injected anti-miR-30a into the inguinal fat pads of DIO mice (Supplementary Fig. 7*A*). Seven days after infection, Adv-anti-miR-30a efficiently decreased *miR-30a* expression in iWAT by 60% (Supplementary Fig. 7*B*). Consistent with our observations in lean mice, the activity of STAT1 was increased in the iWAT of anti-miR-30a–treated mice (Supplementary Fig. 7*C*), as was the expression of proinflammatory genes (Supplementary Fig. 7*D*). The negative effect of anti-miR-30a on lipid metabolism (Fig. 6*I*) genes was corroborated by gene expression analysis of *ADIPOQ*, markers of lipogenesis, and fatty acid oxidation genes (Supplementary Fig. 7*E*).

To determine whether disrupting *miR-30a* influences metabolism and inflammation in vitro, we transfected human adipocytes with inhibitors of *miR-30a*. We found that inhibiting *miR-30a* expression was sufficient to increase protein levels of STAT1, but not STAT2 or STAT3 (Fig. 6*L*). Elevated STAT1 protein levels corresponded with reduced expression of ADIPOQ and CytC, which suggested that miR-30a expression is crucial for maintaining key markers of insulin sensitivity and mitochondrial function (Fig. 6*L*). Additionally, we found that *miR-30a* inhibition significantly induced genes that reflect STAT1 transcriptional activation (*STAT1*, *ISG15*, and *OAS1*) and inflammation (*TNFA*), which coincided with reduced expression of critical metabolic genes (Fig. 6*M*). To determine the impact of these changes on metabolic activity, oxygen consumption was measured. We found that maximal respiration was reduced when human adipocytes were transfected with anti-miR-30a RNAs as compared with anti-control RNAs (Fig. 6*N*). Dampened respiratory capacity correlated with reduced MitoTracker staining and more fragmented structures compared with controls (Fig. 6*O*). Together, these data suggest that *miR-30a* inhibition enables STAT1 to drive an inflammatory program that consequently disrupts metabolic activity in adipocytes.

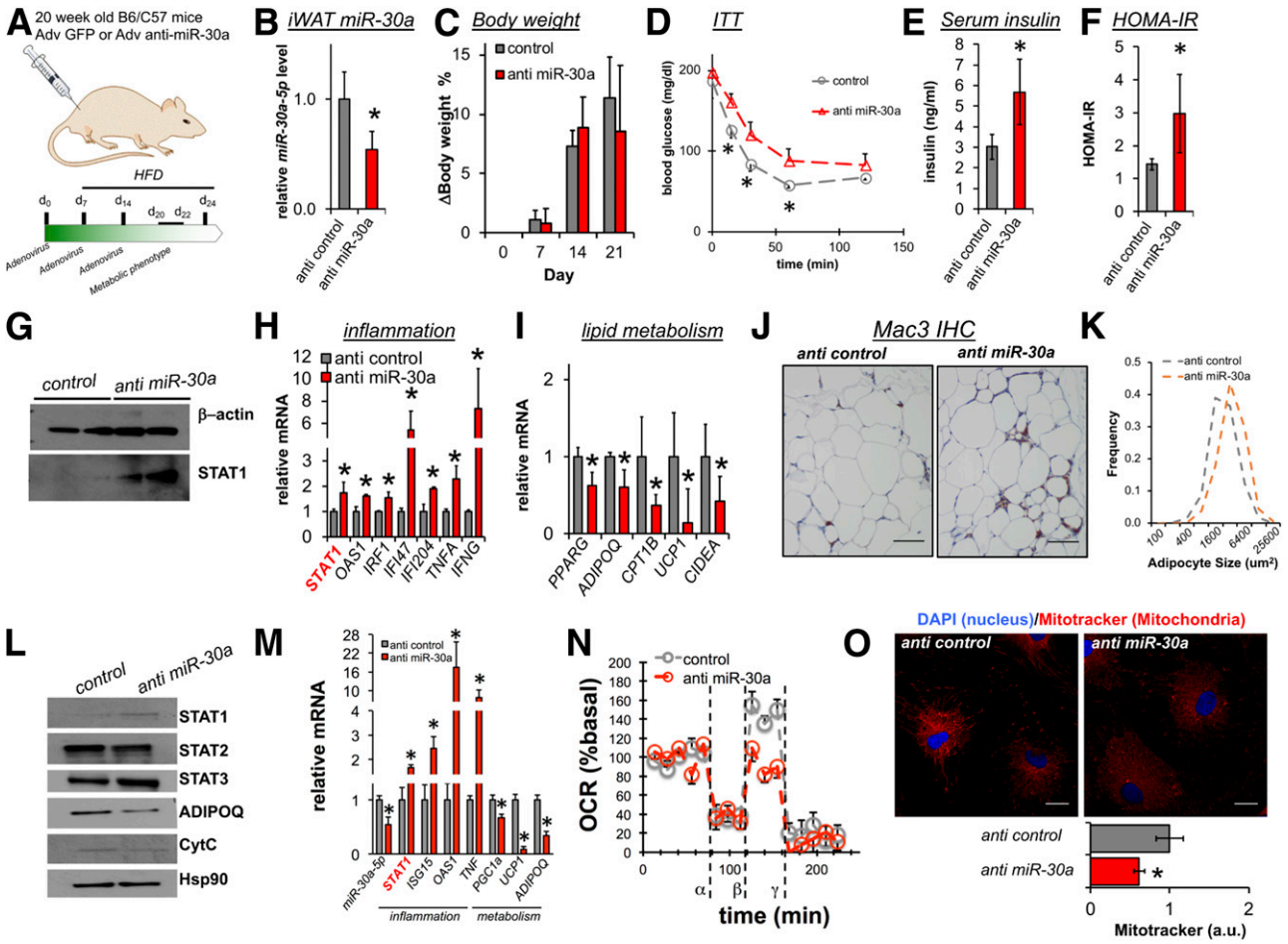

Figure 6—Inhibiting miR-30a in subcutaneous WAT is proinflammatory. *A*: Recombinant Adv vectors expressing GFP scrambled control or miR-30a-5p inhibitor were used for iWAT infection in male 20-week-old mice (n = 4–5/group). *B*: Adv transduction of iWAT was confirmed by qPCR (n = 4–5 ± SEM). *C*: Body weight gain of mice expressing Adv-GFP or Adv-anti-miR-30a in iWAT. *D*: Three weeks after the first injection, glucose metabolism was determined by insulin tolerance tests (ITT; n = 4–5 mice/group). Serum insulin levels (*E*) and HOMA-IR (*F*) were assessed in fasted mice (4 h) injected with Adv-miR-30a or Adv-GFP control (n = 4–5 mice/group). *G*: Western blot analysis of total STAT1 levels in iWAT infected with control or anti-miR-30a Adv. qPCR was used to determine the expression of proinflammatory (*H*) and lipid metabolism (*I*) genes in iWAT (n = 4–5 ± SEM). *J*: Immunohistochemistry (IHC) staining for resident proinflammatory macrophages in iWAT from DIO mice treated with local Adv-GFP or Adv-anti-miR-30a injection. Scale bars, 50 μm. *K*: Adv-anti-miR-30a expression in iWAT increases adipocyte size. *L*: Western blot analysis of STAT1, STAT2, STAT3, ADIPOQ, CytC, and Hsp90 (loading control) in human adipocytes transfected with anti-control or anti-miR-30a single-stranded RNAs. *M*: Expression of *miR-30a*, proinflammatory, and metabolic transcript levels in mature human adipocytes expressing anti-control or anti-miR-30a (representative of three independent experiments). *N*: Respiration (as OCR) was measured in human adipocytes transfected with anti-control or anti-miR-30a. Percent change in OCR (%basal) was normalized to baseline rates (n = 5/group). *O*: Mitochondria (MitoTracker) and nuclei (DAPI) were labeled in human adipocytes transfected with anti-miR-30a as in *L*–*N*. Image analysis was used to determine changes in MitoTracker staining (n = 2 independent experiments, 50–100 cells/experiment). Scale bars, 20 μm. *$P < 0.05$, relative to control transfection. a.u., arbitrary units.

STAT1 and miR-30a Form a Feedback Loop That Enables IFN-γ Sensitivity in Adipocytes

The increase in STAT1 activity upon *miR-30a* depletion suggested that signals that regulate inflammatory responses might impinge upon *miR-30a* expression. Like other genes transcribed by RNA polymerase II, miRNA expression is transcriptionally regulated by conventional transcription factors (29). To date, few miRNAs have been identified as transcription factor targets, but our analysis of genome-wide studies (30,31) predicted that *miR-30a* is a direct target gene of STAT1 and PPAR-γ (Supplementary Fig. 8*A*). In agreement with the genome-wide binding results, in silico analysis nominated STAT1 (GAS) and PPAR-γ binding sites located proximal to the *miR-30a* transcriptional start site. To first determine if PPAR-γ activation affected *miR-30a* expression, we treated mature human adipocytes with rosiglitazone. Rosiglitazone strongly increased the mRNA expression of *ADIPOQ* (Supplementary Fig. 8*B*), *UCP1* (Supplementary Fig. 8*C*), and *miR-30a* (Supplementary Fig. 8*D*), suggesting transcriptional control by PPAR-γ activation. These initial results implied that *miR-30a* is a PPAR-γ target gene.

Among the primary IFNs expressed in the adipose tissue of obese mice, IFN-γ exhibited high expression and sensitivity to Adv-miR-30a injection (Supplementary

Fig. 9). IFN-γ binding to its receptor causes STAT1 homodimerization and binding to GAS sites, leading to transcription of a specific subset of STAT1 target genes that coincides with suppression of both insulin sensitivity and lipid catabolism in adipocytes (32–34). To determine if STAT1 activation affected *miR-30a* expression, we treated mature human adipocytes with IFN-γ, which reduced *miR-30a* expression (Fig. 7*A*) while potently stimulating STAT1 target genes (Fig. 7*B*). Conversely, the expression of metabolic genes critical for insulin sensitivity and lipid metabolism was blunted by IFN-γ (Fig. 7*B*). To further define the transcriptional regulation of *miR-30a*, we investigated how IFN-γ affected the occupancy of PPAR-γ and STAT1 near insulin sensitivity genes and *miR-30a* (Fig. 7*C*). Chromatin immunoprecipitation qPCR revealed that IFN-γ significantly increased binding of STAT1 near the PPAR-γ sites in the *miR-30a* promoter without altering the occupancy of PPAR-γ. We observed the same behavior at *ADIPOQ* (30) and *UCP1* (35) enhancer regions that corresponded with reduced expression of both genes. These findings suggest a negative cross talk between the occupancy of PPAR-γ and STAT1 binding sites near the *miR-30a* gene.

To determine whether expression of *miR-30a* can protect adipocytes against the inhibitory effects of IFN-γ on

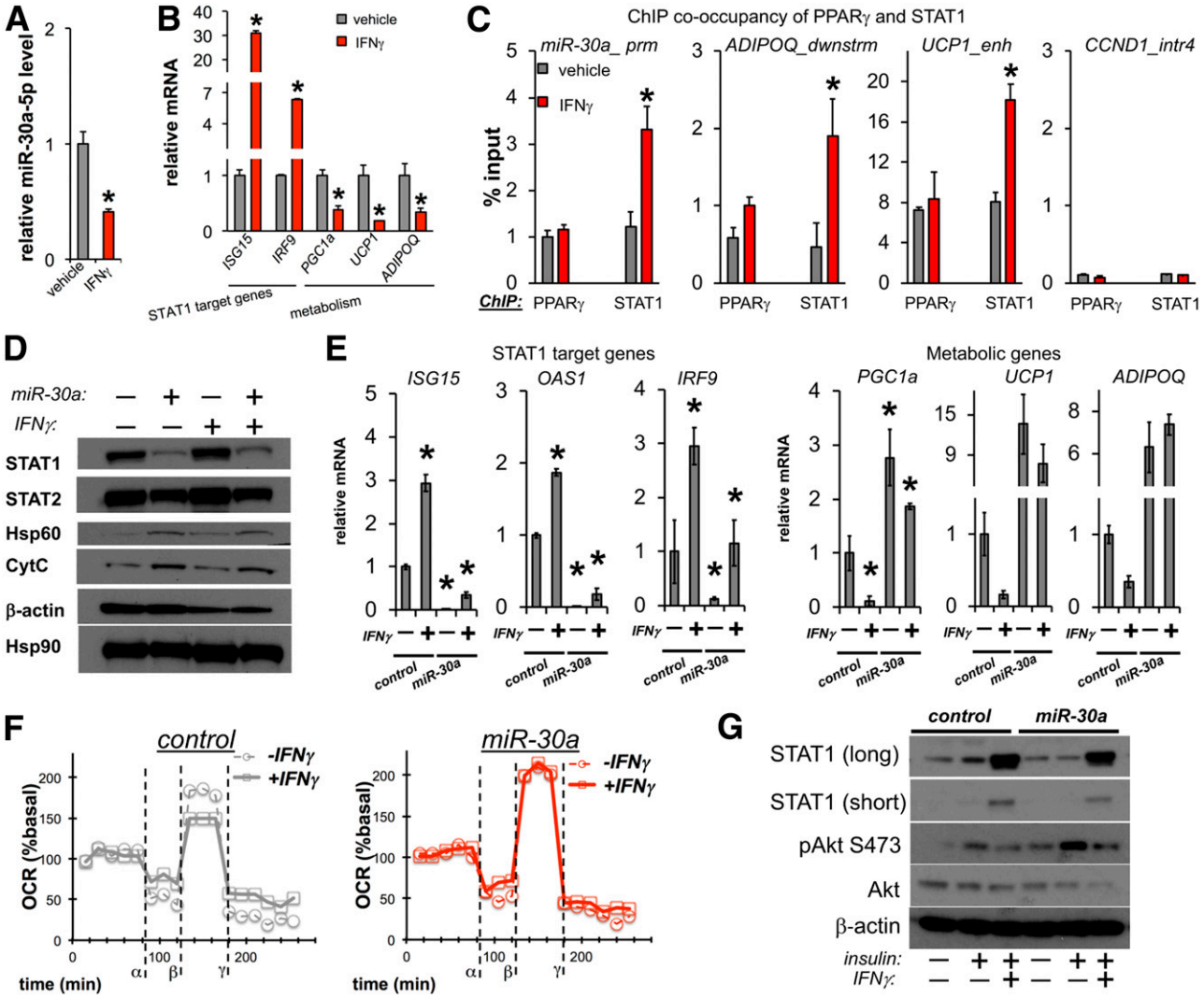

Figure 7—*miR-30a* expression confers resistance to IFN-γ in white adipocytes. Relative mRNA levels of *miR-30a-5p* (*A*) and STAT1 target and metabolism genes (*B*) in human adipocytes treated ± recombinant IFN-γ. *C*: Chromatin immunoprecipitation (ChIP) qPCR analysis of PPAR-γ and STAT1 co-occupancy in human adipocytes treated with 0.1% BSA (vehicle) or recombinant IFN-γ. *D*: Immunoblots of total cell lysates from human adipocytes transfected with control or miR-30a mimic and treated with vehicle or IFN-γ for 10 min. *E*: qPCR analysis of STAT1 target genes and insulin sensitivity genes in cells transfected with control or miR-30a mimic and treated with vehicle or IFN-γ for 24 h. *F*: Respiration (as OCR) was measured in human adipocytes transfected with control or miR-30a mimic and treated with vehicle or IFN-γ for 24 h. Percent change in OCR (%basal) was normalized to baseline rates (n = 5 group). *G*: Immunoblots of total cell lysates from human adipocytes transfected with control or miR-30a mimic and treated with vehicle or IFN-γ for 72 h in serum-free media containing 0.2% BSA. Cells were subsequently exposed to insulin for 7 min in the presence or absence of IFN-γ to assess end points of insulin signaling. *$P < 0.05$, relative to control transfection.

metabolism, we transfected mature human fat cells with control or *miR-30a* mimics followed by treatment with vehicle or IFN-γ. Transient expression of *miR-30a* depleted STAT1 protein levels while only modestly affecting STAT2. Remarkably, mitochondrial proteins that reflect respiratory capacity, including Hsp60 and CytC, were rendered largely insensitive to IFN-γ by overexpression of *miR-30a* (Fig. 7*D*). More broadly, *miR-30a* expression in human adipocytes blocks the induction of STAT1 target genes (*ISG15* and *IRF9*) and allows *PGC1a*, *UCP1*, and *ADIPOQ* expression to be resistant to the effects of IFN-γ treatment (Fig. 7*E*). Metabolic activity of adipocytes transfected with control mimics remained sensitive to IFN-γ, as demonstrated by reductions in maximal OCR. Consistent with metabolic resistance, maximal OCR in human adipocytes was not affected by IFN-γ under conditions of *miR-30a* overexpression (Fig. 7*F*).

Our data suggest that *miR-30a* expression in human adipocytes confers resistance to effects of the proinflammatory IFN-γ on lipid metabolism. Not surprisingly, insulin resistance evolves in adipocytes treated with cytokines like IFN-γ (32,36–38). To test whether *miR-30a* expression preserves insulin signaling in the presence of IFN-γ, we transfected human adipocytes with miR-30a mimics and analyzed insulin-stimulated pAkt after 72-h IFN-γ treatment. Despite chronic IFN-γ treatment, *miR-30a* expression preserved and increased insulin-mediated pAkt (Fig. 7*G*). Control-transfected cells exhibit a blunted response to insulin in the presence of IFN-γ. These results suggest that *miR-30a* can block the effects of proinflammatory STAT1 signaling on the metabolic function of adipocytes.

DISCUSSION

Numerous studies have detailed how the immune compartment within WAT responds to overnutrition, and many cytokines and other soluble mediators of inflammation have been implicated in the metabolic dysfunction that characterizes obesity. In this study, we provide evidence that expression of the miRNA *miR-30a* protects adipocytes from the detrimental effects of proinflammatory cytokines, leading to improved insulin sensitivity in obese mice. Our observations linking *miR-30a* expression in subcutaneous WAT to insulin sensitivity in humans suggest an uncharacterized pathway that may uncouple obesity from the metabolic dysfunction leading to T2DM. Mechanistically, persistent repression of STAT1 activity enables adipocytes to retain metabolic function in the inflammatory environment of obesity and T2DM.

Although the mechanism is unclear, recent work has shown that UCP1-positive adipocytes in WAT may protect against fatty liver and hepatic insulin resistance (39), even without influencing weight gain (40,41). We propose that the metabolic benefits of *miR-30a* in subcutaneous WAT can be partly ascribed to the appearance of UCP1-positive cells in iWAT that do not ultimately impact weight gain. This metabolic gene profile, particularly reflected by UCP1, reflects higher lipid-buffering capacity, which partly explains the lower circulating lipid levels and reduced liver steatosis observed in mice ectopically expressing miR-30a in subcutaneous WAT. The anti-inflammatory effect of *miR-30a* resembles the antidiabetic activity of PPAR-γ agonists like rosiglitazone (42), which also recruit UCP1-positive, smaller adipocytes in subcutaneous WAT. As such, part of the anti-inflammatory activity of PPAR-γ agonists may require *miR-30a* to suppress transactivators downstream of IFN-γ or other cytokines. Not surprisingly, inflammation inhibits generation of UCP1-positive fat cells in subcutaneous WAT (40). Therefore, we expect that *miR-30a* expression in fat cells unites metabolic and anti-inflammatory effects that uncouple obesity from insulin resistance.

Elevated levels of cytokines like IFN-γ (38) characterize the obese environment and consequently impair adipose tissue expandability and attenuate systemic insulin sensitivity. Prominent effects of IFN-γ activation in adipocytes include reduced mitochondrial function and suppression of genes critical for fat metabolism. The mechanism by which *miR-30a* improves insulin sensitivity appears to be mediated by attenuating inflammation derived from IFN-γ in adipose tissue. This result agrees with previous studies showing that IFN-γ disrupts mitochondrial respiration and expression of metabolic genes (32,33,43). Importantly, the inhibitory effects of *miR-30a* on STAT1 appear to be cell autonomous, as reduced *miR-30a* expression allows STAT1 de-repression, elevated IFN-γ signaling, and inhibition of genes important for lipid and glucose homeostasis in adipocytes. In the complex microenvironment of WAT, we found that *miR-30a* also suppresses critical autophagy proteins (22,24), as well as previously established targets, including PI3KCD (44–46) and Ubc9 (12), that correlate with insulin resistance. Further studies will be required to understand how *miR-30a* exerts tissue-specific functions. Along these lines, it will now be important to determine whether *miR-30a* expression blunts the effects of other obesity-related cytokines, such as tumor necrosis factor-α, that exploit STAT1 or other targets to transduce inflammatory signals in adipose tissue.

Inflammation in subcutaneous WAT discriminates obesity from insulin resistance in mice and humans (47). Despite the data linking inflammation to adipose tissue dysfunction, little is known of the mechanisms present that enable expansion of adipose tissue in such a way that protects insulin sensitivity in obesity. We have identified a reciprocal relationship between reduced *miR-30a* expression and STAT1 activation by IFN-γ that advances our understanding as to how inflammatory cytokines impede the normal metabolic function of adipocytes. Our data provide support for the concept that sustained *miR-30a* expression in obesity may disable the IFN-γ signaling pathway and allow fat expansion even under the stress of overnutrition. Additional focus on the role of *miR-30a* in the adipose tissue microenvironment may define new mechanisms for therapeutic intervention that prevent obesity-linked

comorbidities and minimize the long-term clinical burden of T2DM.

Funding. This work was funded by the National Cancer Institute (F30CA196108 [D.A.B.] and R21CA205257 [S.E.M.]), the American Diabetes Association (1-18-JDF-025 [B.Z.] and 1-18-IBS-105 [S.M.H.]), the National Institute of Diabetes and Digestive and Kidney Diseases (R56DK113024 [B.Y.], R01DK110184 [T.D.], K01DK096093 [S.M.H.], R03DK105006 [S.M.H.], R01DK114356 [S.M.H.], P30DK056338 [Texas Medical Center Digestive Disease Center], and P30DK079638 [Baylor College of Medicine Diabetes Research Center]), the MacDonald Fund of the Baylor St. Luke's Medical Center (11RDM002 [M.B.]), the Welch Foundation (R.P. Doherty Jr. Welch Chair in Science, Q-0022 [D.D.M.]), the National Natural Science Foundation of China (91742103 [T.D.] and 81770868), the Innovation-driven Project of Central South University (2017CX011 [T.D.]), the Prostate Cancer Research Foundation (S.E.M.), the Baylor College of Medicine Bridge to Independence Program, the Alkek Center for Molecular Discovery (S.M.H.), the American Heart Association (Beginning Grant-in-Aid 15BGIA25850025 [S.M.H.]), and the Caroline Weiss Law Foundation. The Proteomics and Metabolomics Core Facility is funded by the Cancer Prevention Research Institute of Texas (RP120092).

Duality of Interest. No potential conflicts of interest relevant to this article were reported.

Author Contributions. E.-H.K. and P.K.S. conceived the hypothesis, designed the study, performed the majority of the experiments, contributed to discussion, and edited the manuscript. N.C., L.X., and T.D. performed experiments, contributed to discussion, and edited the manuscript. D.A.B., B.Y., and M.B. contributed reagents and tools for the study, contributed to discussion, and edited the manuscript. B.Z. performed experiments and analyzed data. K.R. and D.P. analyzed data. M.P.H. and C.C. analyzed data, contributed to discussion, and edited the manuscript. X.L., X.C., M.T., D.D.M., and S.E.M. contributed to discussion and edited the manuscript. S.M.H. conceived the hypothesis, designed the study, performed the majority of the experiments, and wrote the manuscript. All authors reviewed the results and approved the final version of the manuscript. S.M.H. is the guarantor of this work and, as such, had full access to all the data in the study and takes responsibility for the integrity of the data and the accuracy of the data analysis.

References

1. Guo F, Garvey WT. Cardiometabolic disease risk in metabolically healthy and unhealthy obesity: stability of metabolic health status in adults. Obesity (Silver Spring) 2016;24:516–525

2. Tomiyama AJ, Hunger JM, Nguyen-Cuu J, Wells C. Misclassification of cardiometabolic health when using body mass index categories in NHANES 2005-2012. Int J Obes 2016;40:883–886

3. Kim JY, van de Wall E, Laplante M, et al. Obesity-associated improvements in metabolic profile through expansion of adipose tissue. J Clin Invest 2007;117:2621–2637

4. Kusminski CM, Holland WL, Sun K, et al. MitoNEET-driven alterations in adipocyte mitochondrial activity reveal a crucial adaptive process that preserves insulin sensitivity in obesity. Nat Med 2012;18:1539–1549

5. Yaghootkar H, Lotta LA, Tyrrell J, et al. Genetic evidence for a link between favorable adiposity and lower risk of type 2 diabetes, hypertension, and heart disease. Diabetes 2016;65:2448–2460

6. Saltiel AR, Olefsky JM. Inflammatory mechanisms linking obesity and metabolic disease. J Clin Invest 2017;127:1–4

7. Dahlman I, Forsgren M, Sjögren A, et al. Downregulation of electron transport chain genes in visceral adipose tissue in type 2 diabetes independent of obesity and possibly involving tumor necrosis factor-alpha. Diabetes 2006;55:1792–1799

8. Hotamisligil GS, Arner P, Caro JF, Atkinson RL, Spiegelman BM. Increased adipose tissue expression of tumor necrosis factor-alpha in human obesity and insulin resistance. J Clin Invest 1995;95:2409–2415

9. Kintscher U, Hartge M, Hess K, et al. T-lymphocyte infiltration in visceral adipose tissue: a primary event in adipose tissue inflammation and the development of obesity-mediated insulin resistance. Arterioscler Thromb Vasc Biol 2008;28:1304–1310

10. Schmidt FM, Weschenfelder J, Sander C, et al. Inflammatory cytokines in general and central obesity and modulating effects of physical activity. PLoS One 2015;10:e0121971

11. Hartig SM, Hamilton MP, Bader DA, McGuire SE. The miRNA interactome in metabolic homeostasis. Trends Endocrinol Metab 2015;26:733–745

12. Koh EH, Chen Y, Bader DA, et al. Mitochondrial activity in human white adipocytes is regulated by the ubiquitin carrier protein 9/microRNA-30a axis. J Biol Chem 2016;291:24747–24755

13. Hartig SM, Bader DA, Abadie KV, et al. Ubc9 impairs activation of the brown fat energy metabolism program in human white adipocytes. Mol Endocrinol 2015;29:1320–1333

14. Mueller M, Thorell A, Claudel T, et al. Ursodeoxycholic acid exerts farnesoid X receptor-antagonistic effects on bile acid and lipid metabolism in morbid obesity. J Hepatol 2015;62:1398–1404

15. Kim D, Pertea G, Trapnell C, Pimentel H, Kelley R, Salzberg SL. TopHat2: accurate alignment of transcriptomes in the presence of insertions, deletions and gene fusions. Genome Biol 2013;14:R36

16. Trapnell C, Williams BA, Pertea G, et al. Transcript assembly and quantification by RNA-Seq reveals unannotated transcripts and isoform switching during cell differentiation. Nat Biotechnol 2010;28:511–515

17. Civelek M, Hagopian R, Pan C, et al. Genetic regulation of human adipose microRNA expression and its consequences for metabolic traits. Hum Mol Genet 2013;22:3023–3037

18. Seale P, Conroe HM, Estall J, et al. Prdm16 determines the thermogenic program of subcutaneous white adipose tissue in mice. J Clin Invest 2011;121:96–105

19. Rydén M, Andersson DP, Bergström IB, Arner P. Adipose tissue and metabolic alterations: regional differences in fat cell size and number matter, but differently: a cross-sectional study. J Clin Endocrinol Metab 2014;99:E1870–E1876

20. Weisberg SP, McCann D, Desai M, Rosenbaum M, Leibel RL, Ferrante AW Jr. Obesity is associated with macrophage accumulation in adipose tissue. J Clin Invest 2003;112:1796–1808

21. Lumeng CN, Bodzin JL, Saltiel AR. Obesity induces a phenotypic switch in adipose tissue macrophage polarization. J Clin Invest 2007;117:175–184

22. Yang Y, Li Y, Chen X, Cheng X, Liao Y, Yu X. Exosomal transfer of miR-30a between cardiomyocytes regulates autophagy after hypoxia. J Mol Med (Berl) 2016;94:711–724

23. Altshuler-Keylin S, Shinoda K, Hasegawa Y, et al. Beige adipocyte maintenance is regulated by autophagy-induced mitochondrial clearance. Cell Metab 2016;24:402–419

24. Yu Y, Yang L, Zhao M, et al. Targeting microRNA-30a-mediated autophagy enhances imatinib activity against human chronic myeloid leukemia cells. Leukemia 2012;26:1752–1760

25. Subramanian A, Tamayo P, Mootha VK, et al. Gene set enrichment analysis: a knowledge-based approach for interpreting genome-wide expression profiles. Proc Natl Acad Sci U S A 2005;102:15545–15550

26. Wu J, Boström P, Sparks LM, et al. Beige adipocytes are a distinct type of thermogenic fat cell in mouse and human. Cell 2012;150:366–376

27. Hamilton MP, Rajapakshe K, Hartig SM, et al. Identification of a pan-cancer oncogenic microRNA superfamily anchored by a central core seed motif. Nat Commun 2013;4:2730

28. Hamilton MP, Rajapakshe KI, Bader DA, et al. The landscape of microRNA targeting in prostate cancer defined by AGO-PAR-CLIP. Neoplasia 2016;18:356–370

29. Corcoran DL, Pandit KV, Gordon B, Bhattacharjee A, Kaminski N, Benos PV. Features of mammalian microRNA promoters emerge from polymerase II chromatin immunoprecipitation data. PLoS One 2009;4:e5279

30. Mikkelsen TS, Xu Z, Zhang X, et al. Comparative epigenomic analysis of murine and human adipogenesis. Cell 2010;143:156–169
31. Robertson G, Hirst M, Bainbridge M, et al. Genome-wide profiles of STAT1 DNA association using chromatin immunoprecipitation and massively parallel sequencing. Nat Methods 2007;4:651–657
32. McGillicuddy FC, Chiquoine EH, Hinkle CC, et al. Interferon gamma attenuates insulin signaling, lipid storage, and differentiation in human adipocytes via activation of the JAK/STAT pathway. J Biol Chem 2009;284: 31936–31944
33. Moisan A, Lee YK, Zhang JD, et al. White-to-brown metabolic conversion of human adipocytes by JAK inhibition. Nat Cell Biol 2015;17:57–67
34. Todoric J, Strobl B, Jais A, et al. Cross-talk between interferon-γ and hedgehog signaling regulates adipogenesis. Diabetes 2011;60:1668–1676
35. Bordicchia M, Liu D, Amri EZ, et al. Cardiac natriuretic peptides act via p38 MAPK to induce the brown fat thermogenic program in mouse and human adipocytes. J Clin Invest 2012;122:1022–1036
36. Houstis N, Rosen ED, Lander ES. Reactive oxygen species have a causal role in multiple forms of insulin resistance. Nature 2006;440:944–948
37. Kang S, Tsai LT, Zhou Y, et al. Identification of nuclear hormone receptor pathways causing insulin resistance by transcriptional and epigenomic analysis. Nat Cell Biol 2015;17:44–56
38. Wentworth JM, Zhang JG, Bandala-Sanchez E, et al. Interferon-gamma released from omental adipose tissue of insulin-resistant humans alters adipocyte phenotype and impairs response to insulin and adiponectin release. Int J Obes 2017;41:1782–1789
39. Cohen P, Levy JD, Zhang Y, et al. Ablation of PRDM16 and beige adipose causes metabolic dysfunction and a subcutaneous to visceral fat switch. Cell 2014;156:304–316
40. Chung KJ, Chatzigeorgiou A, Economopoulou M, et al. A self-sustained loop of inflammation-driven inhibition of beige adipogenesis in obesity. Nat Immunol 2017;18:654–664
41. Hepler C, Shao M, Xia JY, et al. Directing visceral white adipocyte precursors to a thermogenic adipocyte fate improves insulin sensitivity in obese mice. eLife 2017;6:e27669
42. Xu H, Barnes GT, Yang Q, et al. Chronic inflammation in fat plays a crucial role in the development of obesity-related insulin resistance. J Clin Invest 2003;112:1821–1830
43. Kissig M, Ishibashi J, Harms MJ, et al. PRDM16 represses the type I interferon response in adipocytes to promote mitochondrial and thermogenic programing. EMBO J 2017;36:1528–1542
44. Zhong M, Bian Z, Wu Z. miR-30a suppresses cell migration and invasion through downregulation of PIK3CD in colorectal carcinoma. Cell Physiol Biochem 2013;31:209–218
45. Ortega-Molina A, Lopez-Guadamillas E, Mattison JA, et al. Pharmacological inhibition of PI3K reduces adiposity and metabolic syndrome in obese mice and rhesus monkeys. Cell Metab 2015;21:558–570
46. Mauro C, Smith J, Cucchi D, et al. Obesity-induced metabolic stress leads to biased effector memory CD4+ T cell differentiation via PI3K p110δ-Akt-mediated signals. Cell Metab 2017;25:593–609
47. Karelis AD, Faraj M, Bastard JP, et al. The metabolically healthy but obese individual presents a favorable inflammation profile. J Clin Endocrinol Metab 2005; 90:4145–4150